Mathematical Modeling of Single and Multi-Component Adsorption Fixed Beds to Rigorously Predict the Mass Transfer Zone and Breakthrough Curves

Siahpoosh, Mohsen; Fatemi, Shohreh*+; Vatani, Ali

School of Chemical Engineering, University College of Engineering, University of Tehran, P.O.Box 11365-4563, Tehran, I.R. IRAN

ABSTRACT: *The aim of the present work is to prepare an adsorption package to simulate adsorption / desorption operation for both single and multi-component systems in an isothermal condition by different mechanisms such as; local adsorption theory and mass transfer resistance (rigorous and approximated methods). Different mass transfer resistance mechanisms of pore, solid and bidispersed diffusion, together with nonlinear isotherms (Longmuir, Frendlich, Sips and Toth) are taken into account in modeling the fixed bed adsorbers. The Extended Longmuir isotherm was found to explain properly the binary and ternary mixtures in adsorption/desorption process. Almost all the mass transfer approximations were explained by the linear driving force, LDF, although the alternative driving force, ADF, approximation was examined in some cases. The numerical solution was the Implicit Method of Lines which converted the partial differential equations to the ODEs then solving them by the Runge-Kutta method. Validation of the models was performed by the experimental data derived from the literature for different types of adsorbents and adsorbates. The sensitivity analyses was carried out to find out variation of the breakthrough curves against some physical and operational parameters such as; temperature, flow rate, initial and inlet concentration and particle adsorbent size. The results revealed excellent agreement of simulated and previously published experimental data.*

KEY WORDS: *Multicomponent adsorption, Simulation, Mathematical modeling, Breakthrough curves.*

INTRODUCTION

Gas adsorption is widely used for the large scale purification or bulk separation of air, natural gas chemical and petrochemical processes, where it is often better to use gas phase adsorption rather than the older unit operations of distillation or absorption. The dynamic mathematical models are required to simulate the gas adsorption processes, mainly to study the behavior of the new adsorbents during adsorption-desorption cycles and optimization purposes. Adsorption of gas mixtures in the fixed bed columns is the most popular process, because;

* *To whom correspondence should be addressed.*
+ *E-mail: shfatemi@ut.ac.ir*
1021-9986/09/3/25 20/$/4.00

(1) the industrial processes need continuous operations which are easily recognized by the fixed beds in which TSA, PSA, VSA and purge gas swing methods have been proposed for commercial separations, (2) application of fixed bed maintains crushing and dust formation of adsorbents at low level, (3) fixed beds have low utility and maintenance costs [1].

In the past, the design of the adsorbers was carried out empirically through extensive experimentation on process development units; *Yoon* and *Nelson*, [2] developed an empirical model to predict the breakthrough curve of activated carbon beds. These methods are both expensive and time consuming. Another popular method is formulation of the bed and particles in the adsorption system and solving the equations by analytical or numerical methods. In the single component adsorption systems with linear relationship between solid and fluid phase, application of the analytical solution is possible. Although one of the best improved analytical solutions is the constant pattern method which uses the Longmuir isotherm for a binary system of adsorption, there are made some assumptions which have restricted its application [3].

Solution of the multi-component adsorption models with nonlinear equilibrium isotherms including mass transfer resistances and bed axial dispersion must be performed numerically, to solve the derived equations, simultaneously.

Development of the numerical methods helps us to reduce the simplified assumptions in formulation and improve the results of modeling. Since simultaneous solving of the PDEs is tedious and time consumed, use of approximate methods of mass transfer resistance can be accounted for the adsorbent particles.

The most widely used approximated methods is the so-called linear driving force (LDF) approximation that was originally obtained by *Glueckauf* and *Coates* [4] for the surface diffusion mechanism with a constant diffusivity. *Liaw et al.* [5] have shown how LDF is related to the parabolic concentration profile in spherical adsorbent. Generally, in approximated methods the average solid concentration can be calculated by solving only one ODE, therefore the time of calculations can be reduced. Some approximated methods have been introduced by *Carta* and *Cincotti* [6], in which an adsorption film model was presented for diffusion in spherical particles. Also, *Zhang* and *Ritter* [7] treated the case of the parallel pore and surface diffusion resistance, in which they assumed a parabolic profile for the combined pore and solid phase concentrations. *Leinekugel-le-Cocq et al.,* [8] prepared a double LDF model for approximation in the bidispersed adsorbent structures. *Yang* and *Doong* [9] were the first to formulate equations for the bed and adsorbent particle by rigorous solving method, meanwhile in the solution scheme they assumed parabolic concentration inside the particle. Pore and surface diffusion mechanisms in non isothermal conditions have also been investigated by *Serbezov* and *Sotrichos* [10]. More recently, *Sankararao* and *Gupta* [11] have considered the pressure, velocity and temperature variations with axial dispersion in the bed for both approximation and rigorous solving methods with pore diffusion mechanism.

According to the invention of new types of porous materials, molecular sieves and adsorbents, design and simulation of the new processes is required specifically in the field of multi-component separations by different mechanisms of pore, solid and bidispersed diffusion resistances.

Therefore, this work is an attempt to present a general purpose package for mathematical modeling and comparison different mechanisms of rigorous and approximate methods. The models of the presented package are prepared on the base of different forms of local equilibrium and local kinetic theory, lumped and rigorous mass transfer resistance in the particles with macro and/or micropore diffusion controlled mechanisms. The models are solved numerically for different case studies of laboratory and industrial adsober units and they are validated using different experimental data prepared from the literature.

MATHEMATICAL MODELING

The mathematical models are based on the following assumptions:

The gas phase behaves as the ideal gas.

The process is isothermal adsorption.

The mass and velocity gradients are negligible in radial direction of the bed.

The bed is tubular and the axial dispersion is considered in the bulk phase.

The particles are spherical and they are packed uniformly into the fixed bed.

Gas phase pressure is constant; meanwhile the fluid velocity is varying according to the total mass balance along the bed, in the multi-component systems.

Adsorption isotherms are either applicable for single or multi-component systems: Longmuir, Frendlich, Sips and Toth can be used for single component adsoption and extended Longmuir is used for multi-component mixtures.

The popular models available in the literature are divided into two main categories based on local adsorption assumption between the solid and bulk phase or existence of mass transfer resistance between adsorbent particle and fluid phase.

The component mass balance of the bulk phase is derived as the following equation in a packed bed:

$$-D_{z,i}\frac{\partial^2 C}{\partial \zeta^2}+\frac{\partial (uC_i)}{\partial \zeta}+\frac{\partial C_i}{\partial t}+\frac{1-\varepsilon}{\varepsilon}N_i=0 \qquad (1)$$

$$C=\frac{C_i}{C_{0,i}} \quad ; \quad \zeta=\frac{z}{1}$$

Boundary conditions are:

$$\text{B.C.1}: C_1(0,t)=1+\frac{D_{z,i}}{u.l}\frac{\partial C_i(0,t)}{\partial \zeta} \qquad (2)$$

$$\text{B.C.2}: \frac{\partial C_i(l,t)}{\partial \zeta}=0$$

Different adsorption mechanisms are presented in the following sections.

Local adsorption models

Local adsorption assumption relates to the negligible effect of mass transfer resistance through the particles. This model can be used in the systems with high mass transfer rates. According to the rate of adsorption into the solid phase, these models are divided into local equilibrium theory and local kinetic theory.

Local equilibrium theory

This model is expressed by existence of equilibrium between solid and fluid concentration, therefore the volume molar flux of component i, in the bed model, is replaced by the following equation.

$$N_i=\rho_P\frac{q_{0,i}}{C_{0,i}}\frac{\partial q_i^*}{\partial t}=\rho_P\frac{q_{0,i}}{C_{0,i}}\sum_{j=1}^{N}\frac{\partial q_i^*}{\partial C_j}\frac{\partial C_j}{\partial t} \qquad (3)$$

$$q_i^*=\frac{q_i^*}{q_{0,i}}$$

Using the Extended Langmuir isotherm in multi-component systems:

$$q_i^*=\frac{C_{0,i}}{q_{0,i}}\frac{q_{m,i}K_iC_i}{\left(1+\sum_{j=1}^{n}K_jC_{0,j}C_j\right)}$$

for i≠j

$$\frac{\partial q_i^*}{\partial C_j}=\frac{C_{0,i}}{q_{0,i}}\frac{q_{m,i}K_i\left(-K_jC_i\right)}{\left(1+\sum_{j=1}^{n}K_jC_{0,i}C_j\right)^2} \qquad (3\text{-a})$$

and for i=j

$$\frac{\partial q_i^*}{\partial C_i}=\frac{C_{0,i}}{q_{0,i}}\frac{q_{m,i}K_i\left(1+\sum_{\substack{j=1\\ j\neq i}}^{n}K_jC_{0,j}C_j\right)}{\left(1+\sum_{j=1}^{n}K_jC_{0,j}C_j\right)^2} \qquad (3\text{-b})$$

Local kinetic theory

This model is expressed by the kinetic rate isotherm between solid and fluid concentration, therefore N_i is replaced by a rate equation as the following. In this package Longmuir kinetic rate is selected for the local kinetic assumption [12]:

$$R_{ads}=\frac{\partial\theta}{\partial t}=k_a(1-\theta)C-k_d\theta \quad ;\theta=\frac{q}{q_m} \qquad (4)$$

$$N_i=\rho_P\left(k_aC_i(q_m-q_{0,i}q_i)-k_d\frac{q_{0,i}q_i}{C_{0,i}}\right) \qquad (5)$$

The relation of (k_a/k_d) is the equilibrium constant of Longmuir isotherm.

Mass transfer resistance models

On the base of mass transfer resistance between fluid and solid particles, the particle diffusion is considered in

the model by two different types of solution procedure such as approximation and rigorous methods. They are introduced in the following sections.

Approximation solving methods

In these methods, mass transfer resistance is described by a lumped- resistance coefficient and the driving force can be expressed as the difference between fluid or solid-phase concentrations, in either linear (LDF) or alternate (ADF) forms. In the approximation methods only bed formulation is described by the partial differential equation and the average solid concentration appears in ordinary differential equation. The following subsections are different kinds of the approximation procedures.

Pore diffusion mechanism

This mechanism of diffusion usually occurs in the macro or mesoporous adsorbents. The adsorbed flux can be expressed by the either two following forms. The first equation implies that the component accumulates on both pore and solid phases with the local equilibrium between them and the other equation shows only accumulation in the solid phase.

$$N_i = \varepsilon_P \frac{\partial \bar{C}_{P,i}}{\partial t} + \rho_P \frac{q_{0,i}}{C_{0,i}} \frac{\partial \bar{q}_i}{\partial t} \tag{6-a}$$

$$N_i = \rho_p \frac{q_{0,i}}{C_{0,i}} \frac{\partial \bar{q}_i}{\partial t} \tag{6-b}$$

By the LDF approximation and various mass transfer resistances, N_i can be expressed by different formulas. The fluid phase driving force concentration can be used for Eq (6-a) and the solid phase driving force can be used for Eq (6-b) , respectively, in the following formulas.

$$N_i = \frac{\partial \bar{C}_{P,i}}{\partial t}\left(\varepsilon_P + \rho_P \frac{q_{0,i}}{C_{0,i}} \frac{\partial \bar{q}_i}{\partial \bar{C}_{P,i}}\right) = k_i\left(C_i - \bar{C}_{p,i}\right) \tag{6-a′}$$

$$N_i = \rho_p \frac{q_{0,i}}{C_{0,i}} \frac{\partial \bar{q}_i}{\partial t} = k_i\left(q_i^* - \bar{q}_i\right) \tag{6-b′}$$

k_i , which is the lumped mass transfer coefficient, can be expressed by the either form of the following equations:

Internal mass transfer resistance (IMTR):

$$k_i^{int} = \frac{15 D_{p,i}^e \varepsilon_p}{R_p^2} \tag{7}$$

External mass transfer resistance (EMTR):

$$k_i^{ext} = \frac{3 k_{f,i}}{R_p} \tag{8}$$

Overall mass transfer resistance (OMTR)

$$\frac{1}{k_i^{overall}} = \frac{R_p}{3 k_{f,i}} + \frac{R_p^{\,2}}{15 \varepsilon_p D_{p,i}^e} \tag{9}$$

In Eq 6-b', the equilibrium solid concentration $\left(q_i^*\right)$, is related to the bulk concentration $\left(C_i\right)$, by an isotherm equation or the equilibrium factor (β), (*Yang*, 1987),

$$\beta = \frac{C_i(1-q_i^*)}{q_i^*(1-C_i)} \;;\; q_i^* = \frac{C_i}{\beta + (1-\beta) C_i} \tag{10}$$

In the above equation, q_i^* is in equilibrium with C_i. Eq. (10) can be used when the equilibrium factor (β) i s constant. Longmuir isotherm always has a constant equilibrium factor because $\beta_i = 1/(1+K_i)$ for any component, where K_i is the Longmuir equilibrium parameter. There is also an alternative driving force to explain Ni using the constant equilibrium factor (β) as the following [13]:

$$N_i = k_i^{int} \psi_{p,i} \frac{q_i^* - \bar{q}_i}{\left(1 + (\beta - 1)\bar{q}_i\right)^{0.5}} \tag{11}$$

In the above equation $\psi_{p,i}$ is the correction factor, which is $\frac{0.548}{1 - 0.452(\beta_i)^{0.5}}$.

Surface diffusion mechanism

Diffusion in sufficiently small pores, such that the diffusing molecules can never escape the force field of the adsorbent surface is called surface diffusion mechanism. In this mechanism only IMTR model is selected, because the surface diffusivity coefficient is generally much smaller than the other diffusivities [3], it means that IMTR is so higher than EMTR. Since pore radius is very small, it is assumed that all of the adsorbates adsorb on the surface of the adsorbent. In this case only Eq. (6-b) is selected as the flux of the component i, as follow:

$$N_i = \rho_p \frac{q_{0,i}}{C_{0,i}} k_i^s (\bar{q}_i^* - \bar{\bar{q}}_i) \quad (12)$$

$$k_i^s = \frac{15 D_{S,i}^e}{R_p^2} \quad (13)$$

Like the pore diffusion mechanism, it may be possible to choose ADF approximation to describe lumped resistance in the surface diffusion mechanism, such as Eq. (14); [14]:

$$N_i = \frac{\rho_p q_{0,i} \psi_{S,i} k_i^s}{C_{0,i}} \left(\frac{\bar{q}_i^{*2} - \bar{\bar{q}}_i^2}{2\bar{\bar{q}}_i} \right) \quad (14)$$

In the above equation $\psi_{S,i}$ is $\dfrac{0.59}{1-0.41(\beta_i)^{0.5}}$.

Parallel pore & surface diffusion mechanism

Sometimes pore and surface mechanisms compete or corporate together. The dominant mechanism also depends on both adsorbate and adsorbent properties, and operational conditions such as temperature and concentration. Using both diffusivities causes a tedious solving procedure of the rigorous method, while usin LDF approximation is the easiest way of solution. In this mechanism N_i is used from Eq. (6-b) together with the following equations:

$$N_i = \left(k_i^{int} + k_i^s \frac{\rho_p q_0}{C_0} \right) \left(\bar{q}_i^* - \bar{\bar{q}}_i \right) = k_i^{P\&S} \left(\bar{q}_i^* - \bar{\bar{q}}_i \right) \quad (15)$$

$$k_i^{P\&S} = \frac{\rho_p q_{0,i}}{C_{0,i}} \frac{15 D_{S,i}^e}{R_p^2} + \frac{15 \varepsilon_p D_{p,i}^e}{R_p^2} \quad (16)$$

Bidispersed diffusion mechanism

In this case, the macropore and micropore diffusion control mass transfer, simultaneousely. Some adsorbents such as zeolites and CMSs are made by compressing very small crystals, usually with a small percentage of binder. The size order of crystals is 0.1 to 1 micron, although the pellet sizes are in millimeters. Double LDF model is used by *Leinekugel-le-Cocq et al.,* [8] to approximate the mass transfer of the adsorbent. In this situation Eq. (17) would be used for N_i.

$$N_i = \varepsilon_p \frac{\partial \bar{C}_{p,i}}{\partial t} + \rho_p \frac{q_{0,i}}{C_{0,i}} \frac{\partial \bar{\bar{q}}_i}{\partial t} = k_i^{ovrerall} \left(C_i - \bar{C}_{p,i} \right) \quad (17)$$

In which:

$$\frac{\partial \bar{\bar{q}}_i}{\partial t} = \frac{15 D_{S,i}}{R_c^2} \left(\frac{q^*(C_i)}{q_{0,i}} - \bar{\bar{q}}_i \right) \quad (18)$$

where, $\bar{\bar{q}}$ is the dimensionless solid average concentration in the pellet and $\bar{q}$ is the dimensionless average solid concentration in crystal and $k^{overall}$ is replaced by Eq. (9).

Rigorous methods

In these methods the particle diffusion resistance is taken into account by mass balance formulation inside the pores and/or solid phase along the particle radius. Different mechanisms of pore, surface and bidispersed diffusion resistance are derived in this kind of method. In the solution algorithm, the PDEs of the bed and pellet are solved, simultaneously .

Pore diffusion model

In this mechanism, pore diffusion is the main resistance of mass transfer into the particles, and there is local equilibrium within the pore and solid phase at each time. The pore fluid mass balance of the ith component in the spherical particle is as follows:

$$\left(\varepsilon_p + \rho_p \frac{\partial \bar{q}_i}{\partial C_{p,i}} \right) \frac{\partial C_{p,i}}{\partial t} = \quad (19)$$

$$\frac{1}{\left(R_p \Re\right)^2} \frac{\partial}{\partial \Re} \left[\Re^2 \left(\varepsilon_p D_{p,i}^e \right) \frac{\partial C_{p,i}}{\partial \Re} \right]$$

$$C_{p,i} = \frac{C_{p,i}}{C_{0,i}} \quad ; \quad \Re = \frac{r}{R_p}$$

where the boundary conditions are:

$$B.C.1 : \frac{\partial C_{p,i}}{\partial \Re} = 0 \ ; \ \Re = 0$$

$$B.C.2 : \frac{3}{R_p^2 \varepsilon_p D_{p,i}^e} \left. \frac{\partial C_{p,i}}{\partial \Re} \right|_{\Re=1} = k_i^{overall} \left(C_i - C_{p,i} \right) \quad (20\text{-a})$$

$$\text{or} = k_i^{overall} \left(\bar{q}_i^*(C_i) - \bar{\bar{q}}_i \right) \quad (20\text{-b})$$

In above equations the average pore and solid concentration are calculated by the following equations,

in which q_i^* and $\bar{q}_i$ are in equilibrium with $C_i$and $\bar{C}_{p,i}$, respectively:

$$\bar{C}_{p,i} = 3\int_0^1 \bar{C}_{p,i}\Re^2 d\Re \quad (21)$$

$$\bar{q}_i = q(\bar{C}_{p,i})/q(C_{0,i}) \quad ; \quad q_i^* = q\,C_i/q(C_{0,i}) \quad (22)$$

If the mass transfer rate is expressed by the EMTR, the, B.C.2 is replaced by:

$$\frac{3}{R_p^2}\varepsilon_p D_{p,i}^e \left.\frac{\partial \bar{C}_{p,i}}{\partial \Re}\right|_{\Re=1} = k_i^{ext}\left(C_i - \bar{C}_{p,i}\big|_{\Re=1}\right) \quad (23\text{-a})$$

$$\text{or} \quad = k_i^{ext}\left(q_i^*(C_i) - \bar{q}_i^*\big|_{\Re=1}\right) \quad (23\text{-b})$$

According to the driving force in B.C. 2; the first equations (20-a or 23-a) which are defined by fluid phase concentrations are used as Ni in Eq. (6-a) and the second equations (20-b or 23-b) which are based on the solid concentration are used as the flux in Eq. (6-b). Based on these formulas, the rigorous methods of pore diffusion can be expressed by four different boundary conditions, as shown in table 2, (models 14 to 17).

Surface diffusion model

In this model, solid or surface diffusion is the main resistance of adsorption, therefore the particle mole balance equation contains only the solid phase concentration as follows:

$$\frac{\partial \bar{q}_i}{\partial t} = \frac{1}{(R_p\Re)^2}\frac{\partial}{\partial \Re}\left(D_{s,i}^e \Re^2 \frac{\partial \bar{q}_i}{\partial \Re}\right) \quad (24)$$

$$\text{B.C.1}: \frac{\partial \bar{q}_i}{\partial \Re} = 0 \quad (\Re = 0)$$

$$\text{B.C.2}: \frac{3\rho_p q_{0,i}}{C_{0,i}R_p^2} D_{S,i}^e \left.\frac{\partial \bar{q}_i}{\partial \Re}\right|_{\Re=1} = k_i^{ext}\left(q_i^*(C_i) - \bar{q}_i\big|_{\Re=1}\right) \quad (25)$$

In surface diffusion mechanism, N_i is expressed by Eq. (6-b) with the right-hand side of Eq. (25).

Bidispersed diffusion model

In this model both pore and solid diffusion control the mass transfer resistance inside the particles. In this case, three dynamic models of bed, macropores and micropores (crystals) must be solved, simultaneously. In this model, N_i, in Eq. (1), is expressed by:

$$N_i = \varepsilon_p \frac{\partial \bar{C}_{p,i}}{\partial t} + \rho \frac{q_{0,i}}{C_{0,i}}\frac{\partial \bar{q}_i}{\partial t} \quad (26)$$

The mass balance equation within the macropores:

$$\frac{\partial \bar{C}_{p,i}}{\partial t} + \frac{(1-\varepsilon_p)\rho_p q_{0,i}}{\varepsilon_p C_{0,i}}\frac{\partial \bar{q}_i}{\partial t} = \frac{1}{(R_p\Re)^2}\frac{\partial}{\partial \Re}\left[\Re^2\left(D_{p,i}^e\right)\frac{\partial \bar{C}_{p,i}}{\partial \Re}\right] \quad (27)$$

$$\text{B.C.1}: \frac{\partial \bar{C}_{p,i}}{\partial \Re} = 0 \quad (\Re = 0)$$

$$\text{B.C.2}: \frac{3D_{p,i}^e \varepsilon_p}{R_p^2}\left.\frac{\partial \bar{C}_{p,i}}{\partial \Re}\right|_{\Re=1} = k_i^{ext}\left(C_i - \bar{C}_{p,i}\big|_{\Re=1}\right) \quad (28)$$

The mass balance in micropores or crystals:

$$\frac{\partial \bar{q}_i}{\partial t} = \frac{1}{(R_C\delta)^2}\frac{\partial}{\partial \delta}\left(D_{S,i}^e \delta^2 \frac{\partial \bar{q}_i}{\partial \delta}\right) \qquad \delta = \frac{r}{R_C} \quad (29)$$

where the interface crystal concentration is at equilibrium with macropores concentration:

$$\text{B.C.1}: \frac{\partial \bar{q}_i}{\partial \delta} = 0 \quad (\delta = 0) \quad (30)$$

$$\text{B.C.2}: \bar{q}_i\big|_{\delta=1} = \frac{q^*(C_{p,i})}{q_{0,i}}$$

The average solid concentration in Eq. (26) can be replaced by the following equation;

$$\bar{\bar{q}}_i = 3\int_0^1 \bar{q}_i \Re^2 d\Re \quad (31)$$

Pore diffusion with kinetic isotherm

This model is the same as pore diffusion model except that no equilibrium exists between pore and solid. The solid concentration is assumed as a lumped phase and is related to the pore phase by the kinetic form of the adsorption isotherm as the following;

Table 1: The equations for estimation of mass transport and physical parameters.

Molecular diffusivity coefficient, [15]	$D_{i,j}=\frac{T^{15}}{p\sigma_{i,j}^2\Omega}\left(\frac{1}{M_i}+\frac{1}{M_j}\right)^{0.5}\left(0.0027-0.0005\left(\frac{1}{M_i}+\frac{1}{M_j}\right)^{0.5}\right)$ $\sigma_{i,j}=\frac{\sigma_i+\sigma_j}{2}\quad {}^0A \qquad ;\varepsilon_{i,j}=(\varepsilon_i\varepsilon_j)^{0.5}$ $\Omega_D=(44.54(k_BT/\varepsilon_{i,j})^{-4.909}+1.911(k_BT/\varepsilon_{i,j})^{-1.575})^{0.1}$ $\varepsilon/k=0.75T_C \qquad ;\sigma=0.841V_C^{1/3}$
Molecular diffusivity in mixture, [15]	$D_{m,i}=\frac{1-y_i}{\sum_{x=j}^{n}\frac{y_i}{D_{i,x}}}$
Knudsen Diffusivity coefficient, [3]	$D_{k,i}=9.7\times10_{rp}^3(\frac{T}{M_i})^{0.5}$
Bosanquet equation, [3]	$D_{p,i}^e=\frac{1/\tau}{(1/D_{m,i})+(1/D_{K,i})}$
Axial dispersion coefficient [16]	$\frac{\varepsilon D_{z,i}}{D_{m,i}}=20+0.5ScRe \quad Re=\frac{\rho u\varepsilon d_p}{\mu_m};Sc=\frac{\mu_m}{\rho D_{m,i}}$
External mass transfer coefficient, [16]	$Sh=\frac{k_{f,i}\,d_p}{D_{m,i}}=2+1.1\left(\frac{\mu}{\rho D_{m,i}}\right)^{\frac{1}{3}}\left(\frac{d_pG}{\mu}\right)^{0.6}=2+1.1sc^{1/3}\,Re^{0.6}$
Tortuosity factor, [17]	$\tau_p=\varepsilon_p+1.5(1-\varepsilon_p)$
Viscosity of pure gas, [18]	$\mu=\frac{AT^B}{(C+D/T+E/T)}$
Viscosity of gas mixture, [19]	$\mu=\sum_{i=1}^{n}\frac{y_i\mu_i}{\sum y_i\Phi_{i,j}} \quad ; \quad \Phi_{i,j}=\frac{1}{\sqrt{8}}\left(1+\frac{M_i}{M_j}\right)^{-\frac{1}{2}}\left[1+\left(\frac{\mu_i}{\mu_j}\right)^{\frac{1}{2}}\left(\frac{M_j}{M_i}\right)^{\frac{1}{4}}\right]^2$

$$\varepsilon_p\frac{\partial \bar{C}_{p,i}}{\partial t}+\rho_p\left(k_a\bar{C}_{p,i}(q_{m,i}-q_{0,i}\bar{q}_i)-k_d\frac{q_{0,i}\bar{q}_i}{C_{0,i}}\right)= \quad (32)$$

$$\frac{1}{(R_p\Re)^2}\frac{\partial}{\partial\Re}\left[\Re^2(\varepsilon_pD_{p,i}^e)\frac{\partial \bar{C}_{p,i}}{\partial\Re}\right]$$

Contact boundary condition of the particle and bulk phase of the bed is expressed by the Eq. (23-a).

In order to solve the proposed mathematical models, mass transport coefficient and physical parameters were predicted according to the correlations existing in the literature. These equations are summarized in table1.

Numerical procedure

The set of PDEs is solved using the numerical method of lines [20]. The method of lines is a convenient technique for solving time dependent partial differential equations. In this method, all the spatial derivatives are replaced by the finite difference method, whereas the time derivatives left intact. In fact, this is an explicit time-stepping finite difference algorithm in which the time step determined automatically and adaptively by the ODE solver. Therefore, PDEs of the bed and particles in rigorous methods, and bed PDEs in the approximated methods are converted into the system of ODEs. This package is programmed in MATLAB software 7 (The Mathworks, Inc) in three layers of calculations.

In the first layer, all of the input data are imported; a suitable discussed model is selected; all mass transfer parameters are calculated; furthermore at the end of calculations the results are reflected to this layer for reporting or plotting. The second layer is a transporter layer in which all of the required data are transported to

Table 2: Chart of all mathematical models prepared in this package.

Local adsorption models	Local equilibrium theory, Eq. (3)		Extended Longmuir, Longmuir Frendlich, Sips (F-L), Toth			model 1
	Local kinetic theory		Kinetic form of Longmuir, Eq. (5)			model 2
Mass transfer resistance models	Approximation method (Lumped resistance, only bed modeling)	Fluid phase driving force*, Eq. (6-a)	IMTR, Eqs. (6-a′), (7)			model 3
			EMTR, Eqs. (6-a′), (8)			model 4
			OMTR, Eqs. (6-a′), (9)			model 5
			Double LDF, Eqs. (17), (18), (9)			model 6
		Solid phase driving force, Eq. (6-b)	IMTR	Pore diffusion, Eq. (7)	LDF, Eq (6-b′)	model 7
					ADF, Eq (11)	model 8
				Surface diffusion, Eq. (13)	LDF, Eq (12)	model 9
					ADF, Eq (14)	model 10
				Parallel Pore & Surface, Eq.s (15), (16)		model 11
			EMTR, Eqs. (6-b′), (8)			model 12
			OMTR, Eqs. (6-b′), (9)			model 13
	Rigorous method (Bed and Particle modeling)	Pore diffusion mechanism, Eq. (19)	Particle boundary condition	Fluid phase driving force, Eq. (23-a)		model 14
				Solid phase driving force, Eq. (23-b)		model 15
				Fluid phase driving force, Eq. (20-a)		model 16
				Solid phase driving force, Eq. (20-b)		model 17
			Kinetic form of Longmuir, Eq. (33)			model 18
		Surface diffusion mechanism	Eqs. (24), (25)			model 19
		Bidispersed diffusion mechanism	Eqs (26-32)			model 20

**) In the duble LDF which is used for bidispersed adsorbents, Eqs. (17) and (18) are applied instead of Eq. (6-a).*

the solver of the selected model. Also the results of the modeling are returned from the calculation core to the upper layer by this part. The third layer (calculation core) is the ODE solver. In this package the ODE solver is the ODE23tb that is proper for stiff systems that use crude error tolerances [21]. This solver is an Implicit Rung-Kutta method with a first stage that is a trapezoidal rule step and second stage that is a backward differentiation formula of second order. By construction, the same iteration matrix is used in evaluating both stages. All unknown variables must be solved simultaneously in one system of ODEs. The total number of equations, including boundary conditions depends on the respective model. If we define the number of components as N, the number of bed length division is C and the number of particle step size is R; the total number of equations which should be solved by the local equilibrium model (model 1) is N(C+1), for local kinetic model (model 2) it is 2NC, for approximated models of pore, surface and parallel pore & surface diffusion mechanisms (models 3-5 and 7-13) it is 2NC, for approximation model of bidispersed diffusion mechanism (model 6) there is [N(3C-1)] points, while in the rigorous models of the pore and surface diffusion mechanisms (models 14-17 and 19) it has [N(C+1)+N(C-1)(R+1)] points and for the rigorous model of the bidispersed diffusion mechanism (model 20) there is [N(C+1)+N(C-1)(R+1)+N(C-1) (R-1)(E+1)+N(C-1) (R-1)] unknown variables in which E is the number of step sizes inside the crystal.

All the derived models are tabulated in table 2. The first column presents the models divided into two main categories based on MTR mechanism. In the second column, models are detached based on the equilibrium and non equilibrium assumptions, the solving methods,

the fluid or solid phase driving force and the mechanisms of diffusion. The employed equations are presented in the second and third columns and the models are numbered in the last column.

RESULTS AND DISCUSSION

In order to validate the proposed models, eight case studies were selected from different articles and the experimental breakthrough curves were compared with the numerical results of this work. The absolute average deviation (AAD) of non-dimensional output concentrations was introduced as the error term between the experiment and model as the following equation:

$$AAD = \frac{1}{n}\sum_{i=1}^{n}\left|\frac{C_{exp} - C_{model}}{C_0}\right| \quad (33)$$

Where n is the number of data points. In a laboratory scale, if $AAD \leq 0.05$, the results could be highly consistent, If $AAD < 0.1$, data would be probably consistent and if $AAD > 0.1$, the results are not consistent [22].

In this work, five series of the single component adsorption systems, two series of the binary adsorption and a system of the ternary adsorption are studied for several adsorbents such as: activated carbon, activated alumina, CMS, Zeolite 4A and Soil.

The operational conditions and model parameters of the case studies are presented in table 3. Furthermore, the sensitivity analysis of each model was performed and studied at different operational conditions.

Single component Adsorption

Cases one to five are about single component adsorption systems. Meanwhile, the mechanism of adsorption is different, because the compatible models may be varied from one to another.

The first case is the water vapor removal from ethanol vapor by the cornmeal adsorbents [23]. Due to strong polar attraction between water molecules and hydroxyl groups of the adsorbent, water can adsorb faster and stronger than ethanol, therefore this system is considered as a single component adsorption. In this case, because of linearity of the adsorption isotherm of dilute water concentration, the breakthrough curve can be derived analytically [1]. The experimental results are compared with the numerical results of three different models in Fig. 1. In the present case, the porosity of adsorbent is 0.55. The models 3 and 4 are derived on the base of approximation LDF method for internal and external mass transfer resistance, respectively, and the model 14 is presented by the rigorous method on the base of pore diffusion mechanism. The enlarged breakthrough curves at initiation and AAD of each model are presented in this figure. Although model No.14, shows higher accuracy with 6.6 % AAD, the model NO. 3 is recommended with 7.4 % AAD, because of its higher calculation rate. In this case study, the EMTR is 5.9×10^{-4} s, which is much lower than the IMTR 0.946 s, therefore IMTR is the main resistance of diffusion and model 3 is preferred rather than model 4. Fig. 2 is a comparison between model 3 and 4 when changing the particle radius by a factor of one over four. Reduction the adsorbent radius causes decreasing both MTRs, meanwhile the IMTR is much more affected by the particle size. As a result, Fig. 2 shows both models 3 and 4 to approach to each other whenever the IMTR is reduced.

Fig. 3 exhibits the sensitivity analysis for temperature and flow velocity. As shown in this figure, increasing temperature and inlet velocity causes lower breakthrough time. The molecular and Knudsen diffusion coefficients increase by the power of 1.5 and 0.5 over temperature, respectively, and diffusion rate improves in higer temperatures. On the other hand, the adsorption capacity and adsorption constant decrease along the temperature and cause faster bed loading.

The next examination is the adsorption of volatile contaminants on soil in a single component adsorption system [24]. These components are toluene, n-hexane and chlorobenzene. In these examples, nitrogen is the carrier gas and breakthrough curves are expressed by the volume of nitrogen passed through the bed. The adsorbent, bed and operational conditions are expressed in table 3. Since the porosity of the adsorbent is very small, 0.1, the bulk accumulation of particle pores is negligible and the mass flux through the particles is calculated by Eq. (6-b). In this example, the tortuosity factor of the adsorbent is 6 for calculating the effective diffusivity.

In Fig. 4.a, the rigorous solving method and LDF approximation are compared with the experiments. In this figure, breakthrough curve of toluene is plotted by the three models. The breakthrough curve of model 7 shows better confirmation at higher outlet concentrations, while the rigorous model, No. 15, is close to experimental data

Table 3.a: Required parameters for the simulating case studies.

No	Components	Adsorbent	T (K)	P_T (KPa)	C_0 (mol/m^3)	Equilibrium Isotherms Parameters	L(m)	U (m/Sec)	R_P (m)	D_{Bed} (m)
1	Water Vapor	Corn meal	355 364 373	105.5 106.7 109.8	5.1	Henry: K=0.448 K= 0.346 K=0.297	0.2 0.43 0.43	4.2×10^{-2} 5.6×10^{-2} 5.6×10^{-2}	2.25×10^{-4}	2.5×10^{-2}
2	N-Hexane	Soil	297	101.3	1.24	LM: q_m=0.0405 K= 0.838	0.25	4×10^{-2}	1.15×10^{-4}	7.75×10^{-3}
	Toluene				0.355	LM: q_m=0.1026 K= 1.319		21×10^{-3}		
	Chlorobenzene				0.108	Toth: q_m=0.0765 T=0.423, K=150		11.5×10^{-4}		
3	Propane	CMS	343	100	35	Toth: q_m=1.757 T=0.356, K=2.91	0.165	0.2×10^{-3}	1.1×10^{-3}	9.3×10^{-3}
4	Benzene	Activated Carbon	303	101.3	132×10^{-3}	LM: qm= 5.89 K=40 Ka= 1.6×10^{-2} m^3/molSec Kd=4.4×10^{-4} l/Sec	0.031	0.2	1.5×10^{-3}	1.5×10^{-2}
5	Styrene	Alumina active	283	-	6.7	Henry: K=0.3	0.282 0.141 0.07	8.4×10^{-4}	1×10^{-3}	0.033
6	Nitrogen Oxygen	CMS	294	101.3	32.7 8.7	$q_m=2.64\times10^3$ (mol/m^3) $K=3.37\times10^{-3}$ $q_m=2.64\times10^3$ (mol/m^3) $K=3.51\times10^{-3}$	0.7	3.8×10^{-2}	5×10^{-6}	3.5×10^{-2}
7	Methane Ethane	Activated Carbon	298	304	1.3 7	EX.L: q_m=1.86 $K=2.96\times10^{-2}$ q_m=2.87 $K=11.43\times10^{-2}$	0.288	6×10^{-2}	1×10^{-3}	5×10^{-3}
8	Benzene Toluene P-Xylene	Activated Carbon	303	101.3	1636 (ppm) 967 (ppm) 683(ppm)	EX.L: q_m=3.737 K=52.8 q_m=4.208 K=302.6 q_m=3.645 K=1823.5	0.1	0.891	5×10^{-4}	0.0182

concentrations. In this case, the ratio of IMTR to EMTR is 140. It means that the approximation method with EMTR is a poor assumption for the modeling.

Comparison between the ADF and LDF approximation is exhibited in Fig. 4.b. In these methods the equilibrium solid concentrations are estimated by the constant equilibrium factor derived from Longmuir isotherm. In this case, the AAD for LDF approximation is 2.5 % while it is 2 % for the ADF, therefore results of these approximations are close together and there is not any advantage for using ADF method.

Adsorption of chlorobenzene on soil is very favorable while breakthrough times of previous components are very low. This time is 2750 sec for chlorobenzene, while it is 200 and 500 sec for n-hexane and toluene, respectively. This fact could be shown clearly by plotting the bulk concentration of chlorobenzene versus dimensionless length of the bed in Fig. 4.c. It is clearly visible that the mass transfer zone, MTZ is very sharp even at the end of the bed.

The third case is the adsorption of propane on CMS 4A (Takeda Chem. I nd. Lda., Japan) which has a

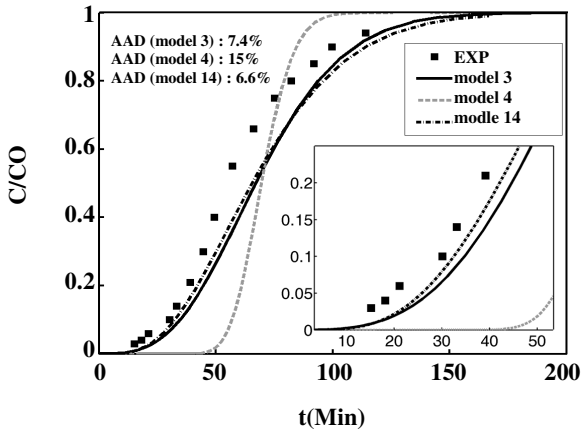

Fig. 1: Breakthrough curves for water vapor adsorption on cornmeal by three different models (T_{bed} = 355 K, R_P = 0.225 mm).

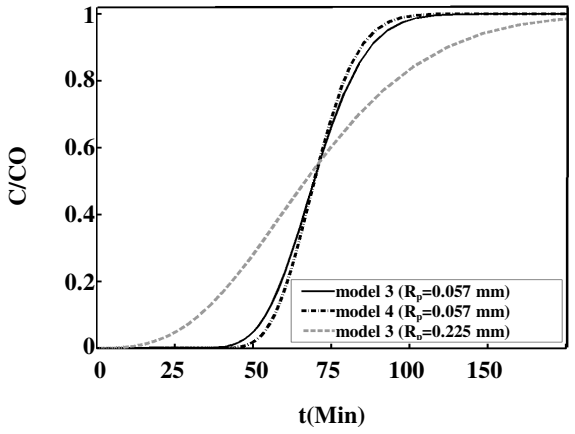

Fig. 2: Sensitivity analysis of breakthrough curve for different particle radius.(T_{bed} = 355 k).

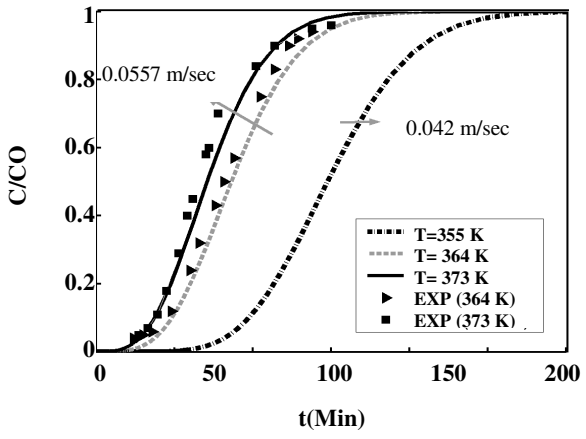

Fig. 3: Validation and sensitivity analysis of model 3 for different temperatures and inlet velocities. (R_p = 0.225 mm, L = 0.43 m).

bi-dispersed structure, therefore after diffusion to the pellet the solute would diffuse through the micro crystals [25]. The MTR of the crystal is the main resistance for diffusion [8], although all types of mass transfer resistances have been accounted in this case, (the MTR in crystal is 769 sec., the IMTR in the pellet is 0.09 sec. and the EMTR is 0.02 sec). The tortuosity factor is 6 and the porosity of the macro pores is 0.315.

In Fig. 5, the breakthrough curves of different models have been plotted to find out which model is closer to the experimental data. The models are introduced as the rigorous method for bidispersed diffusion mechanism, model 20, the double LDF method, model 6, the LDF method for surface diffusion mechanism ,model 9, the LDF method for parallel pore & surface diffusion mechanism, model 11, and the LDF method for pore diffusion mechanism, model 3.

It is evident that the models 6 and 20 are more consistent than the others because these two models, are compatible with the structure of CMS. The double LDF solving method, model 6, reduces time of calculation but rigorous method, model 20, shows closer results to the experimental data (AAD of model 6 is 7.2 %, while it is 5.5 % for model NO. 20). It seems Model 3 is not an efficient procedure for modeling this adsorbent because usually in bidispersed adsorbents the crystal surface diffusion resistance is more than the macro pore resistance, therefore models 6 and 9 show the same precision. Model 11 which uses parallel pore and surface diffusion is not appropriate, because it assumes both mechanisms in parallel, while the structure and the adsorption mechanism of these adsorbents does not follow this regime

By application of the rigorous calculation method, the solid concentration in different radius of the crystal and the average solid concentration of crystals in different radius of the adsorbent pellet are determined. In this case, the solid concentration is a function of four positions as $q(\delta,\Re,\zeta,t)$, in which the first and second variables are the dimensionless radial coordinates in the crystal and pellet, respectively, the third one is the dimensionless length of the bed and the fourth variable is the time. For example in Fig. 6.a the dimensionless solid concentration is observed in two position of crystal in the middle of the particle radius $\Re$=0.5 and in the middle of the bed ξ=0.5 at different times. For any time, the solid

Table. 3.b: Continuous of table 3.a.

No	ε	ρ_p (kg/m^3)	ρ_g (kg/m^3) [a]	μ_g (kg/m.Sec) [a]	D_m(m^2/Sec)[a]	D_k(m^2/Sec)	D_z(m^2/Sec)	D^e(m^2/Sec)	K_f(m/Sec)[a]
1	0.3	847	1.482 1.455 1.431	1.197×10^{-5} 1.226×10^{-5} 1.137×10^{-5}	1.658×10^{-5} 1.726×10^{-5} 1.809×10^{-5}	_	0.00011 a	6.4×10^{-9} 5×10^{-9} b 4.3×10^{-9}	0.127 0.142 0.148
2	0.4	2250	1.37	1.69×10^{-5}	1.017×10^{-5}	_	1.36×10^{-4} b	1.34×10^{-6} b	0.0809
			1.16	1.77×10^{-5}	1.0352×10^{-5}		7.14×10^{-5} b	1.37×10^{-6} b	0.106
			1.47	1.74×10^{-5}	1.01×10^{-5}		3.85×10^{-4} b	1.33×10^{-6} b	0.091
3	0.283	900	0.4316	2.19×10^{-5}	2.35×10^{-5}	8.11×10^{-5}a	0.00166 a	$D_p^e: 3.1\times10^{-6}$ a $D_s^e: 8.4\times10^{-17}$	0.03
4	0.58	880	1.118	1.79×10^{-5}	7.5×10^{-5}	_	4.2×10^{-4} b	6.2×10^{-5} a	0.0392
5	0.453	823	802	_	3.4×10^{-7}	2.5×10^{-7} b	2.9×10^{-7} b	9.47×10^{-9} b	3.8×10^{-4}
6	0.4	1735	_	_	_	_	_	6.101×10^{-9} b	_
7	0.4	_	1.18	2.2×10^{-5}	2.774×10^{-5}	1.57×10^{-4} 1.47×10^{-4}	–	$D_s^e: 6.5\times10^{-14}$ $D_s^e: 5\times10^{-16}$ b	–
8	0.45	946	3.3	1.8×10^{-5}	5.1×10^{-6} 3.4×10^{-6}	–	4.4×10^{-4} 3×10^{-4}	4.25×10^{-6} a 2.9×10^{-6}	0.027 0.02
9	0.44	720	1.146	1.69×10^{-5}	1.19×10^{-5} 1.05×10^{-5} 0.96×10^{-5}	3.82×10^{-7} 3.52×10^{-7} 3.27×10^{-7}	7.48×10^{-4} 7.52×10^{-4} a 7.59×10^{-4}	1.14×10^{-8} 1.05×10^{-8} b 0.957×10^{-8}	0.792 0.714 0.692

a) Calculated parameters by prepared package. b) Parameters are taken from the reference articles.

concentration at δ=0.25 is smaller than that in the crystal surface (δ=1) as shown in the figure. The average pellet concentration is also exactly the same as the average crystal concentration as it is observed. It is concluded that average concentrations of the crystals are equal within the particle, because the IMTR and EMTR have very small effects on the crystal diffusivity. This conclusion is agreed well with the LDF approximation assumption for the surface diffusion mechanism. Fig. 6.b shows that concentration profile of macro pores is uniform while it is variable at any crystal radius, because the macro pore MTR is much less than the crystal MTR. This fact is confirmed by calculation of the solid concentration at different crystal radiuses and different particle radiuses at any time of operation. The case four is focused on the modeling of benzene adsorption onto the activated carbon [12]. For plotting the breakthrough curves of this case, the time of adsorption is converted into dimensionless form on the base of retention time. The retention time is introduced as the following:

$$t_0=(LA-\omega/\rho_p)/Q \qquad (34)$$

Where Q is the volumetric gas flow rate and *w* is the weight of adsorbent (2 g). In this case the porosity of adsorbent is 0.6 and the tortuosity factor is 1.2 which are shown inTable1. Three basic models are compared in this case; the mass transfer resistance model (model 13), local kinetic model (model 2) and local equilibrium model (model 1). Only bed modeling is considered for this case and the results are exhibited in Fig. 7.

Among the models, LDF approximation with OMTR (model 13) showed the best agreement with experimental data. It is also clear that local equilibrium model (model 1) is less accurate with 14 % AAD. This error would increase when the sorbent size is increased more than 40-60 mesh [3], However, the kinetic form of the Longmuir's isotherm (model 2) has shown small deviation from experimental data.

When the particle radius is decreased the experimental results and MTR model (model 13) approaches to the local equilibrium model (model 1) and takes apart from model 2. In fact, mass transfer resistance is dependent to the particle radius in MTR models (such as model 13). This fact is revealed in comparison of the curves of Fig. 6 with the left hand side of Fig. 7 in which model 13 can achieve to model 1.

Variation of the fluid velocity reveals similar effects in both models 1 and 2. Both models use average solid concentration $(\bar{q})$ in the modeling, therefore decreasing the velocity of the bulk fluid increases contact time between adsorbent and fluid to uniformly distribute the component inside the adsorbent particle where the model validity can be increased. Furthermore model 1 follows the local equilibrium theory and decreasing the velocity causes enough contact time to approach to the equilibrium state and more agreement of model 1 and 2 is achieved. The results are shown in Fig. 8, by decreasing the velocity from 0.2 to 0.1 m/sec.

Prediction of the breakthrough curve in liquid adsorption system is also possible by the prepared package, while the physical parameters should be determined by the proper equations. The fifth case is about styrene drying by the activated alumina in the liquid phase [26]. The Equilibrium isotherm and other required parameters are presented in table 3. The breakthrough curves for different bed depth are compared with experimental date in Fig. 9. All breakthrough curves have been plotted by model 7 with their acceptable AADs.

Effect of particle size on the shape of breakthrough curve has been studied in Fig 10.a and 10.b. The broader breakthrough curves are derived by increasing the particle radius, because of enhancing the IMTR. It means that the bulk fluid passes through the bed with low efficiency and more unused bed length. The curves of Fig. 10.a have the same operating conditions; the stoichiometric

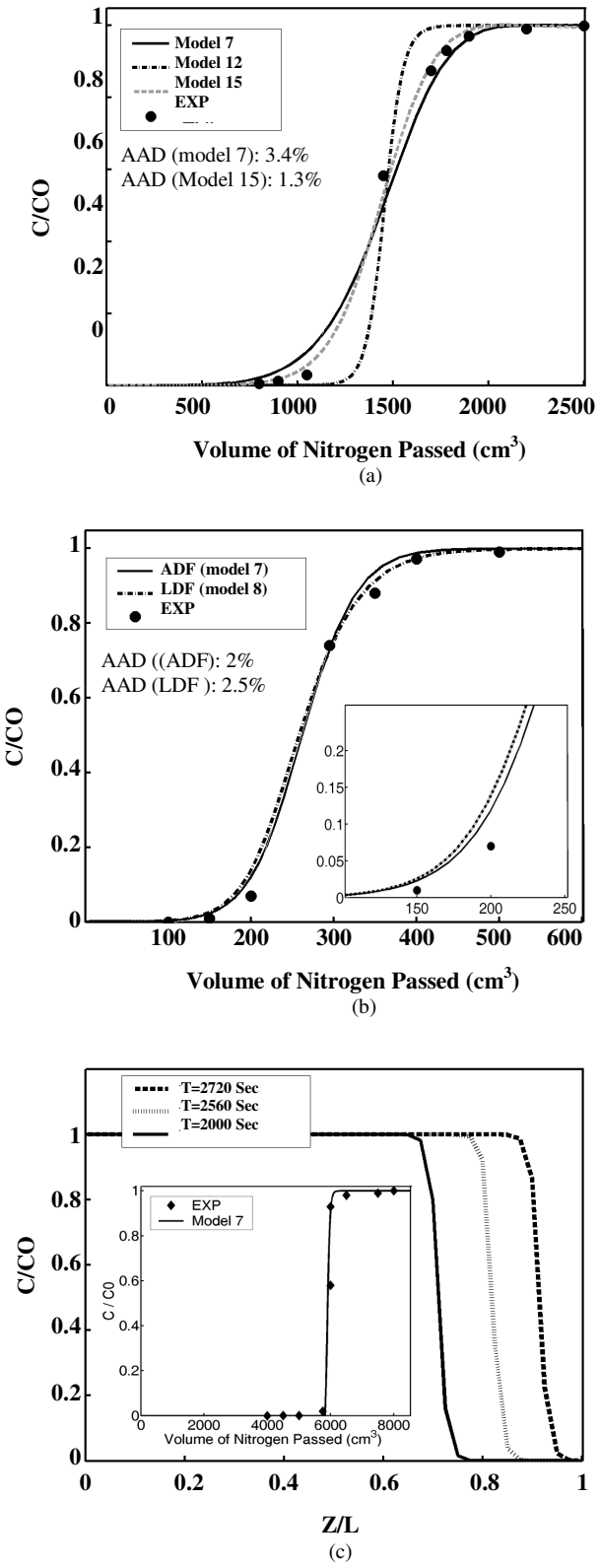

Fig. 4: Breakthrough curves for case two. (a) Adsorption of Toluene, (b) Adsorption of N-hexane, (c) MTZ for different times and breakthrough curve for Chlorobenzene.

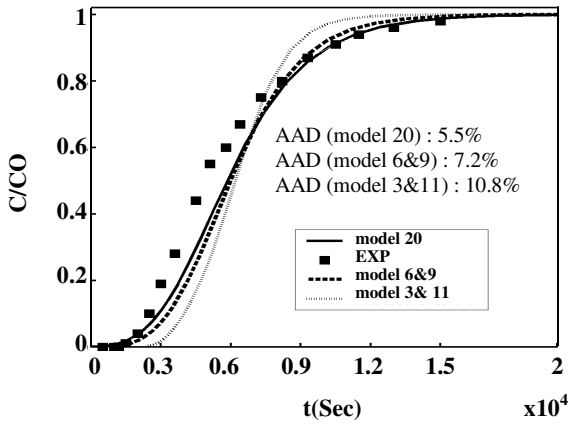

Fig. 5: Breakthrough curves of propane adsorption on CMS (4A) for different models

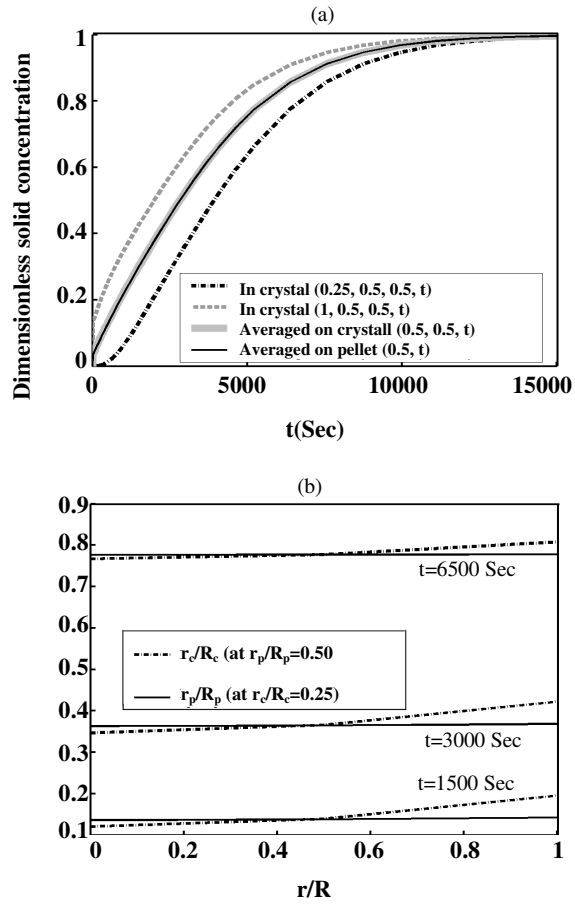

Fig. 6: Propane adsorption on CMS (4A), plotted by model 20. (a) Dimensionless solid concentration in the crystal $q(\delta,R,\zeta,t)$, dimensionless averaged solid concentration in the crystal $q(R,\zeta,t)$ and in the pellet $q(\zeta,t)$ versus time of operation, (b) Solid concentration $q(\delta,0.5,0.5,t)$ versus crystal radius and solid concentration $q(0.25,R,0.5,t)$ versus pellet radius at different times.

time (L/U_{wave}) is equal and this time is approximately 70 hr. The collision point of the curves shows stoichiometric time of bed saturation and the breakthrough curves are extended symmetrically around this point. The stoichiometric wave is an idealized wave for travelling the MTZ through the bed. Fig. 10.b shows the dimensionless average solid concentration versus dimensionless length of the bed at three different times and two different particle sizes. It is clear that the collision point could be disappeared around 70 hr. For the lengths less than collision point, average solid concentration of 1 mm particle size is greater than 2 mm particle size because the smaller radius causes lower MTR and narrower adsorption wave with higher solid concentration.

In conclusion, in the single component adsorption systems with different mechanisms and models (Pore, Solid and etc …) the rigorous models are suggested if high accuracy is required and if EMTR is comparable to IMTR, use of the rigorous methods with OMTR is recommended, while the approximation methods conclude fairly good results with high calculation rate. If velocity of the fluid is low enough using the local kinetic models (models 2 and 18) and local equilibrium models (model 1) conclude acceptable results, meanwhile the local equilibrium model is limited to apply for the small particle radius.

Multi-component Adsorption

In this section three cases of multi-component were investigated. The bulk air separation, adsorption of methane and ethane in the air stream and adsorption of three-component aromatics are studied and compared with mathematical model. The Extended Longmuir isotherm where applied as the equilibrium relation in these case studies

In the case of nitrogen and oxygen separation by CMS [27], the pore distribution of the adsorbent showed micropore morphology and the small effective diffusivity of the components confirmed existence of the solid or micropore diffusion resistance. As it was shown in Fig. 5, for very small surface diffusivity comparing to the pore diffusivity, the main MTR is occurred within the crystal and the diffusion model has a good compatibility by the bidispersed diffusion mechanism such as model 9. The effective solid diffusivity of O_2 (5×10^{-16} m^2/sec) is

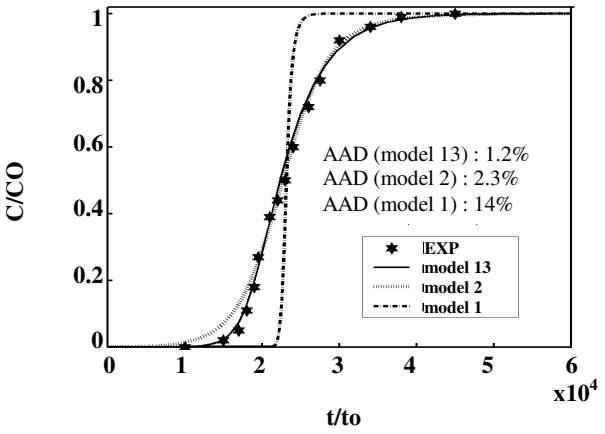

Fig. 7: Comparison of the different models for breakthrough of benzene on activated carbon. particle radius ;1.5 mm and fluid velocity; 0.1 m/sec.

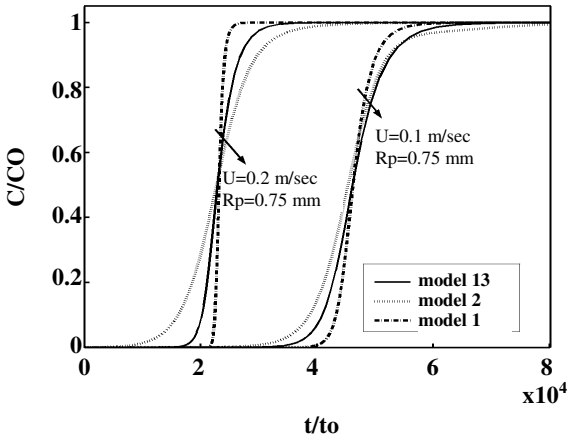

Fig. 8: The sensitivity analysis for changing adsorbent particle radius from 1.5 (base case) to 0.75 mm and changing fluid velocity from 0.2 (base case) to 0.1 m/sec.

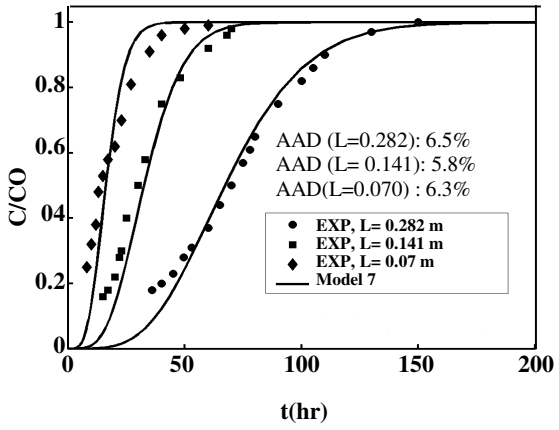

Fig. 9: The breakthrough curves for different bed lengths in purification of styrene from water stream.

hundred times greater than N_2 (6.5×10^{-14} m^2/sec), with no significant difference between their equilibrium parameters, therefore the mechanism of separation is kinetically controlled. Fig. 11 shows the breakthrough curves of N_2 and O_2 in which N_2 exits earlier because of the greater diffusional resistance into the solid phase. Furthermore, the figure shows "roll-up" phenomenon for N_2 concentration profile. This phenomenon is usually observed in multi-component adsorption for both equilibrium and kinetically controlled systems [27].

In these systems, modeling at variable fluid velocities is desirable to approach to the real experimental results. In Fig. 11 the breakthrough curves were calculated at variable and constant velocities and compared with the experiments. The model with variable bed velocity could better confirm the experimental results.

Zeolites 4A is another molecular sieve which can be used for the air separation [28]. In this system the adsorption equilibrium parameter of nitrogen is more than oxygen (For O_2; $q_m=1.77\times 10^4$ mol/m^3 and $k=122.3\times10^{-6}$ m^3/mol, For N_2; $q_m=1.2\times10^4$ mol/m^3 and $k=354\times10^{-6}$ m^3/mol). On the base of adsorption rate constant, O_2 is expected to leave the bed faster than nitrogen, while it is opposed to our expectation and the system is kinetically controlled as the previous case by diffusion resistance because solid diffusivity of oxygen is about hundred times greater than nitrogen (For O_2; 2.24×10^{-15} and for N_2; 2.13×10^{-13} m^2/s). By mathematical model, these two adsorbents have been compared for nitrogen production from air in Fig. 12 at the same conditions mentioned in table 3. The bed with 4A zeolite shows a breakthrough time at 30 sec, whereas, 30 % of the bed is still unused in CMS.

The mechanism of adsorption is pore diffusion; because the effective diffusivities are the same order of molecular diffusivities. In Fig. 13, the breakthrough curves are presented by models 3 and 7 , both of each derived by LDF with IMTR. In model 3, solid adsorption and pore accumulation terms are included, in which the solid average concentration is in equilibrium with the pore average concentration, while model 7 is derived only by the solid adsorption term and it means that diffused molecules, into the particles, would be adsorbed without any accumulion inside the pores. It is evident that model 3 can predict the results better than model 7 as well as the roll up behaviour of the weak adsorbate (methane),

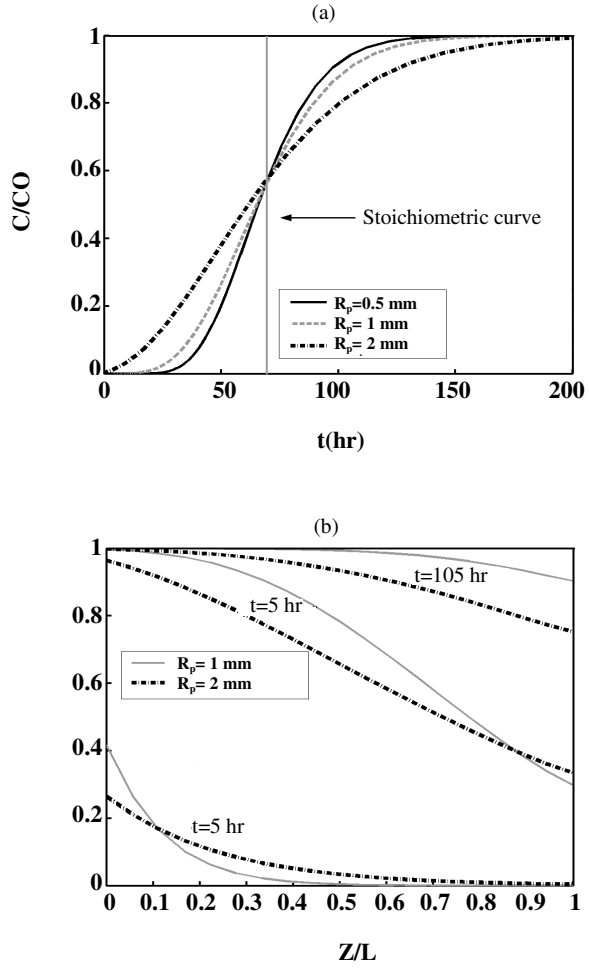

Fig. 10: System of styrene drying, plotted by model 7 (a) Breakthrough curves for different particle radius in L = 0.282 m. (b) $\bar{q}/q^*(c_0)$ ***versus bed length at different times and particle size.***

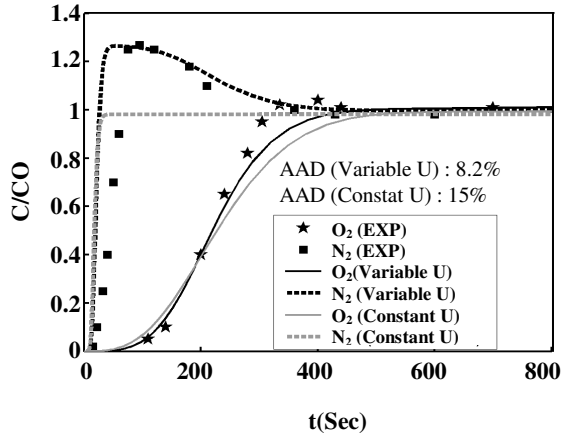

Fig. 11: The breakthrough curve of air on CMS at 1 atm pressure and 294 K, plotted by model 9, for two cases: (1) Constant velocity of the fluid, (2) variable velocity along the bed.

therefore the authenticity of model 3 is acceptable for this experiment.

The sensitivity of the model to the inlet or initial concentrations of methane and ethane is examined in Fig. 14 (a-c). The inlet concentrations of each component is assumed equal. Fig. 14-a shows that increasing the inlet concentrations, accelerates bed saturation and breakthrough curves occure faster with higher roll-up of methane.The results revealed dependency of the roll-up concentration to both velocity and inlet concentration.

The breakthrough curves of desorption stage can be determined by solving the same adsorption model except than verifying the inlet and initial concentrations. By changing the bed dimensionless initial concentration of the adsorption model from 0 to 1 and inlet concentration from 1 to 0, the desorption breakthrough curves by inert gas purge can be derived and plotted in Fig. 14. b. Higher desorption rate is observed in a bed with more initial concentration, because the driving force between adsorbed phase and inert purge gas is larger. For better comprehension of this subject, average solid concentration for different bed initial concentration is plotted in Fig.14. c. for the middle of the bed. It is concluded that a bed with higher initial concentration is more rapidly desorbed.

The last studied case is a ternery-component adsorption process of benzene, toluene and p-xylene in activated carbon [30, 31]. The most required model parameters are estimated from table 3, and other parameters such as tortuosity factor and particle porosity have been taken from the literature as 10 and 0.67, respectively.

The breakthrough curves are plotted in Fig. 15.a, using model 3 with AAD of 7 %. This model could be a good choice for prediction of multicomponent breakthrough curves because of its higher calculation rate and good precision.

Sensitivity of the model investigated for increasing the effective pore diffusivity by decreasing the tortuosity factor from 10 to 5. Fig. 15.b, shows that MTZ of stronger adsorbed species, p-xylene, is shortened because of the higher diffusivity rate into the particles. For the weaker adsorbates, roll up is occurred in MTZ of the bed. Decreasing the tortuosity or/and increasing the effective diffusivities boarden the roll up shapes of the weak adsorbates.

Discussion about selection proper model in the multi-component systems is the same as the single component

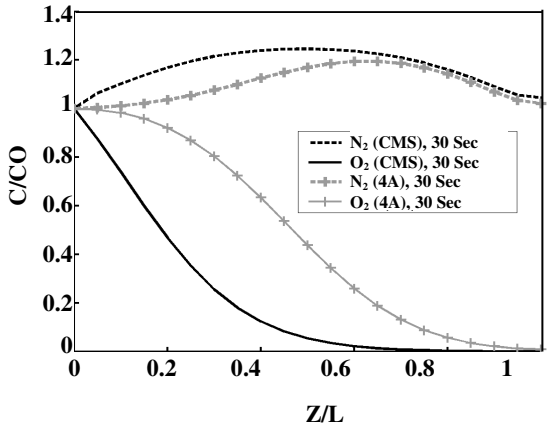

Fig. 12: MTZ for N_2 and O_2 in CMS and Zeolite 4A in the same conditions of Table 3, plotted by model 9.

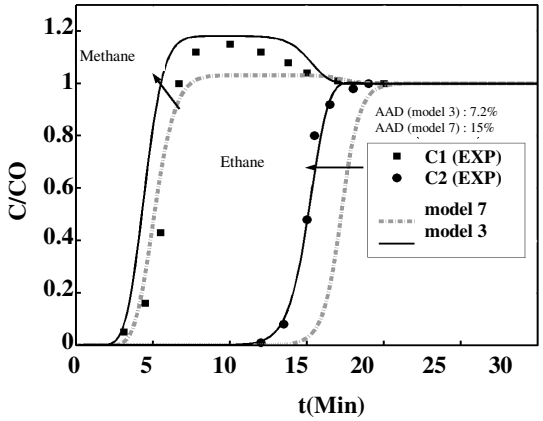

Fig. 13: Comparison two different models by experiment data for Breakthrough curves of methane and ethane on CC818M

system, while in large scale and commercial cases use of the LDF method is recommended because rigorously methods are tedious and time consuming

in the multi-component systems. Some cases, using the pore diffusion mechanism, Eq. (6-a), show better confirmation with experimental data. In these cases accumulation term in the particle has been accounted in bed modeling, which assumes $\bar{q}$ is in equilibrium with $\bar{C}_p$. This model is not true for some cases such as rapid adsorption (high macropore diffusivity) systems or micropore adsorbents

CONCLUSIONS

A comprehensive dynamic mathematical model with numerical solution of multicomponent adsorption in either gas and liquid phases have been developed for simulation of packed bed adsorption process. The developed models are appropriate for design and analysis of fixed bed adsorbers treating multicomponent gas or aqueous mixtures. The numerical package consisting of three major mechanisms of local adsorption, mass transfer approximation and rigorous diffusion controlled with 20 sub-models which take into account the effects of bed axial dispersion, inter, intraparticle and overall mass transfer resistances. The model can predict experimental mass transfer zone and breakthrough curves in adsorption and desorption mode for different adsorbents and molecular sieves such as activated carbon, alumina, zeolites and carbon molecular sieves. The outlet results of the developed models have shown good agreement with the experimental results in various case studies.

This paper is the first work that gathered and compared various mechanisms of mass transfer into the adsorbers for further studies on design and simulation of different adsorption processes, and this package can be readily extended to cyclic operations such as PSA and VSA for industrial case studies.

Nomenclatures

C_i	Bulk concentration of *i* component in the gas phase, (mol/m^3)
$C_{0,i}$	Bulk concentration of *i* component in the inlet gas phase, (mol/m^3)
$\bar{C}_i$	Dimensionless bulk concentration of i component, ($C_i/C_{0,i}$)
$C_{p,i}$	Pore concentration of i component, (mol/m)
$\bar{C}_{p,i}$	Dimensionless pore concentration of i component, ($C_{p,i}/C_{0,i}$)
$\bar{\bar{C}}_{p,i}$	Dimensionless average pore concentration of i component, $\bar{C}_{p,i}/C_{0,i}$
D_p^e	Effective pore diffusivity, (m^2/sec)
D_S^e	Effective solid diffusivity, (m^2/sec)
$D_{z,i}$	Axial dispersion coefficient of i component, (m^2/sec)
d_P	Diameter of the adsorbent particle $2\times R_P$, (m)
K_i	Adsorption equilibrium constant of i component, (m^3/mol)
k_i	Mass transfer coefficient of i component, (1/sec)

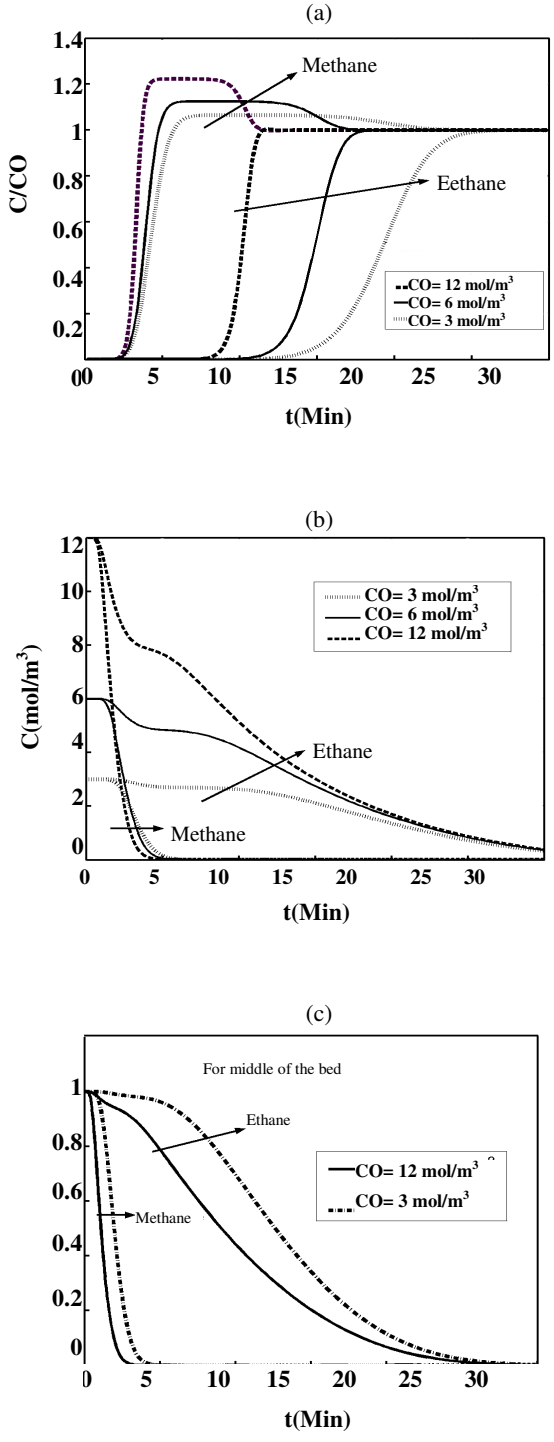

Fig. 14: Effect of inlet concentration on adsorption and desorption of Methane and Ethane by model 3. (a) Breakthrough curves of adsorption in different inlet concentrations. (b) Breakthrough curves of desorption for different initial concentrations. (c) Averaged solid concentration at the middle of the bed for different initial concentration during desorption operation.

k_B	Boltzman constant, 1.38×10^{-23} (J/K)
$k_{f,I}$	External mass transfer coefficient of i component, (m/sec)
k_a	Adsorption constant, (m^3.mol/sec)
k_d	Desorption constant, (1/sec)
l	Bed length, (m)
M	Molecular weight
N_i	Volume molar flux of *i* component, between the gas phase and adsorbent particle, mol/(m^3.sec)
P	Pressure, (kpa)
q_i	Solid concentration of *i* component, (mol/kg)
q_i^*	Equilibrium solid concentration of i component, (mol/kg)
$\overline{q}_i^*$	Dimensionless equilibrium solid concentration of i component, $\left(q_i^*/q_{0,i}\right)$
$\overline{q}_i$	Dimensionless average solid concentration of i component, $\left(\overline{q}_i/q_{0,i}\right)$
$\overline{\overline{q}}_i$	Dimensionless average solid concentration of i component in adsorbent with bidispersed structure, $\overline{\overline{q}}_i = 3\int_0^1 \overline{q}_i d\Re$
$q_{0,i}$	Solid concentration of i component, in equilibrium with $C_{0,i}$, (mol/kg)
$q_{m,i}$	Maximum solid concentration of i component, (mol/kg)
r	Radius distance, (m)
R_C	Radius of the adsorbent particle, (m)
R_P	Temperature, (K)
T	Temperature, (K)
t	Time
t_0	Retention time
u	Interstitial velocity of gas fluid, (m/sec)
V_C	Critical volume in table 1, (cm^3/mol)
z	Axial position in the bed, (m)

Greek letters

β	Equilibrium factor
δ	Dimensionless of crystal radius, (r/R_C)
δ	Collision diameter, (°A)
ε	Interparticle void fraction of bed
ε_P	Pellet void fraction
μ_g	Gas viscosity, (kg/m.sec)
θ	Surface coverage, (q/q_m)

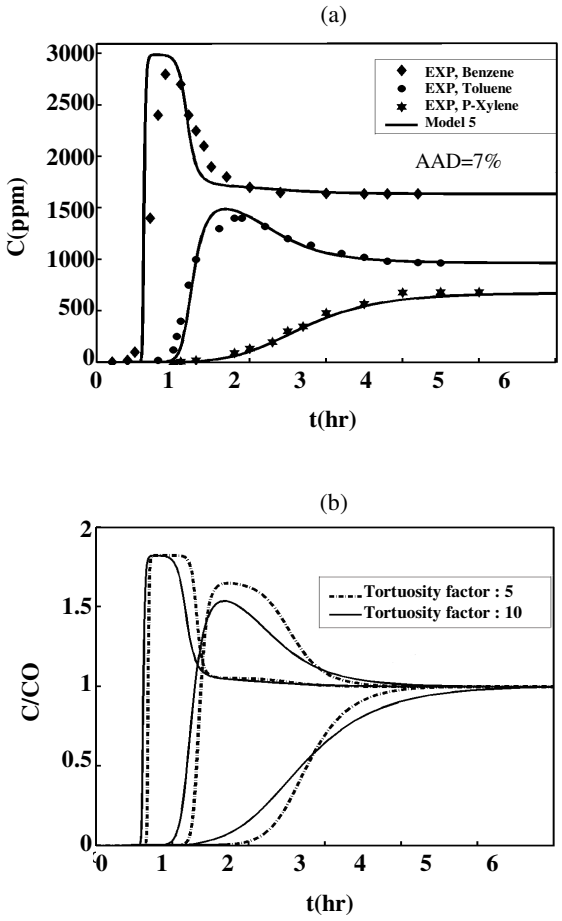

Fig. 15: Adsorption of the benzene, toluene and P-xylene on activated carbon. (a) Comparison by experiment data. (b) Effect of tortuosity factor on breakthrough curves.

ρ_g	Gas phase density, (kg/m^3)
ρ_p	Adsorbent particle density, (kg/m^3)
τ	Tortuosity of macro pores in adsorbent particle
Ω_D	Diffusion collision in Table 1
$\Re$	Dimensionless of particle radius, (r/R_P)
ζ	Dimensionless length of the bed, (z/l)
$\psi_{p,i}$	Correction factor for pore diffusion mechanism in ADF equation
$\psi_{s,i}$	Correction factor for surface diffusion mechanism in ADF equation

Super and Subscripts

e	Effective diffusivity condition
ext	External mass transfer resistance
i, j	i or j component
int	Internal mass transfer resistance
overall	Overall mass transfer resistance
P	Pore
P&S	Parallel pore and solid

Received : 10th February 2008 ; Accepted : 13th April 2009

REFERENCES

[1] Seader, J.D., Henley, E.J., "Separation Process Principles", John Wiley & Sons, Inc., Chap. 15 (2002).

[2] Yoon, Y.H., Nelson, J.H., Application of Gas Adsorption Kinetics: I. A Theoretical Model for Respirator Cartridge Service life, *Am. Ind. Hyg. Assoc. J*., **45** (8), 509 (1984).

[3] Yang, R.T., "Gas Separation by Adsorption Processes", Butterworth's, Boston (1987).

[4] Glueckauf, E., Coates, J.E., *J. Chem. Soc*., 1315 (1947), "Chemical Engineers' Handbook", Perry R.H. and Chilton, C.H.; 7th Ed., Chap 16, New York, McGraw-Hill, (1999).

[5] Liaw, C.H., Wang, J.S.P., Greenkorn, R.H. and Chao, K.C., Kinetics of Fixed-Bed Adsorption: A New Solution, *AIChE. J*., **54**, 376 (1979).

[6] Carta, G., Cincotti, A., Film Model Approximation for Non-Linear Adsorption and Diffusion in Spherical Particles, *Chem. Eng. Sci*., **53**, 3483 (1998).

[7] Zhang, R. and Ritter, J.A., New Approximate Model for Nonlinear Adsorption and Diffusion in a Single Particle, *Chem. Eng Sci*., **52**, 3161 (1977).

[8] Leinekugel-le-Cocq, D., Tayakout-Fayolle, M., Gorrec, Y., Jallut, C., A Double Linear Driving Force Approximation for Non-Isothermal Mass Transfer Modeling Through Bi-Disperse Adsorbents, *Chem. Eng. Sci.*, **62**, 4040 (2007).

[9] Yang, R.T., Doong, S.J. Gas Separation by Pressure Swing Adsorption: A Pore-Diffusion Model for Bulk Separation, *AIChE. J.*, ***31***, 1829 (1985).

[10] Serbezov, A., Sotirchos, S.V., Particle-Bed Model for Multicomponent Adsorption-Based Separations: Application to Pressure Swing Adsorption, *Chem. Eng. Sci*., **54**, 5647 (1999).

[11] Sankararao, B., Gupta, S.K., Modeling and Simulation of Fixed Bed Adsorbers (FBAs) for Multi-Component Gaseous Separations, *Computesr & Chemical Eng*., **31**, 1282 (2007).

[12] Chuang, C.L., Chiang. P. C., Chang, E.E., Modeling VOCs Adsorption onto Activated Carbon, *Chemosphere*, **53**, 17 (2003).

[13] Vermeulen, T., Quilici, *Ind. Eng. Chem. Fundam*., **9**, 179, (1970), "Chemical Engineer's Handbook", (Perry, R.H. and Chilton, C.H., 7th Ed., Chap 16, New York: McGraw-Hill, 1999).

[14] Vermeulen, T., *Ind. Eng. Chem*, **45**, 1664, (1953); "Chemical Engineer's Handbook", Perry, R.H. and Chilton, C.H., 7th Ed., Chap 16, New York: McGraw-Hill, (1999).

[15] Bird, R.B., Stewart, W.E., Lightfoot, E.N., "Transport Phenomena", 2nd Ed., John Wiley & Sons, Inc., New York (2002).

[16] Wakao, N., Funazkri, T., Effect of Fluid Dispersion Coefficients on Particle-Fluid Mass Transfer Coefficients in Packed Bed, *Chem. Eng. Sci.,* **33**, 1375 (1978).

[17] Suzuki, M., Smith, J.M., Axial in Beds of Small Particles, *Chem. Eng. J.,* **3**, 256 (1972).

[18] Daubert, T. E., Danner, R. P., "Physical and Thermodynamic Properties of Pure Chemicals: Data Compilation", New York: Design Institute for Physical Property Data, American Institute of Chemical Engineers/Hemisphere, (1989).

[19] Poling, B.E., Prausnitz, J.M.,O'Connell, J.P., The Properties of Gases and Liquids, 5th Ed., New York, McGraw-Hill, (2001).

[20] Schiesser, W.E., "The Numerical Method of Lines", Academic Press, California, USA (1991).

[21] Kiusalaas, J., "Numerical Methods in Engineering with MATLAB" Cambridge University press (2005).

[22] Lucas, S., Calvo, M.P., Palencia, C., Cocer, M.J., Mathematical Model of Supercritical CO_2 Adsorption on Activated Carbon, Effect of Operating Conditions and Adsorption Scale-Up, *J. of Supercritical Fluids*, **32**, 193 (2004).

[23] Chang, H., Yuan, X., Tian, H., Zeng, A., Experiment and Prediction of Breakthrough Curves for Packed Bed Adsorption of Water Vapor on Cornmeal, *Chem. Eng and Pro*., **45**, 747 (2006).

[24] Thibaud-Erkey, C., Guo, Y., Erkey, C., Akgerman, A., Mathematical Modeling of Adsorption and Desorption of Volatile Contaminants from Soill, *Environ. Sci., Techno*, **30**, 2127 (1996).

[25] Grande, C.A., Silva, M.T.M., Gigola, C., Rodrigues, A.E., Adsorption of Propane and Propylene onto Carbon Molecular Sieve, *CARBON*, **41**, 2533 (2003).

[26] Rivero, M.J., Ibanez, R., Ortiz, I., Mathematical Modeling of Styrene Drying by Adsorption onto Activated Alumina, *Chem. Eng. Sci*., **57**, 2589 (2002).

[27] Farooq, S., Ruthven, M., Dynamics of Kinetically Controlled Binary Adsorption in a Fixed Bed, *AIChE. Journal*., **37**, 299 (1991).

[28] Haas, O.W., Kapoor, A., Yang, R.T., Confirmation of Heavy Component Roll-Up in Diffusion-Limited Fixed Bed Adsorption, *AIChE Journal*., **34**, 1913 (1988).

[29] Siddiqi, K.S., Thomas, W.T., The Adsorption of Methane-Ethane Mixtures on Activated Carbon, *Carbon,* **20**, 473 (1982).

[30] Yun, J. H., Choi, D. K., Kim, S. H., Equilibria and Dynamics for Mixed Vapors of BTX in an Activated Carbon Bed, *AIChE. J.*, **45**(4), 751 (1999).

[31] Gupta, K., Verma, N., Removal of Volatile Organic Compounds by Organic Condens, (2002).